Journal of the Korean Ceramic Society
Vol. 53, No. 1, pp. 43~49, 2016.

http://dx.doi.org/10.4191/kcers.2016.53.1.43

Review

Mixing Rules of Young's Modulus, Thermal Expansion Coefficient and Thermal Conductivity of Solid Material with Particulate Inclusion

Yoshihiro Hirata† and Taro Shimonosono

Department of Chemistry, Biotechnology, and Chemical Engineering, Kagoshima University, Kagoshima 890-0065, Japan

(Received December 21, 2015; Revised January 22, 2016; Accepted January 22, 2016)

ABSTRACT

This review paper analyzed a Young's modulus (E), a thermal expansion coefficient (TEC, β) and a thermal conductivity (κ) of the material with simple cubic particulate inclusion using two model structures: a parallel structure and a series structure of laminated layers. The derived β equations were applied to calculate the β value of the W-MgO system. The accuracy was higher for the series model structure than for the parallel model structure. Young's moduli (E_c) of sintered porous alumina compacts were theoretically related to the development of neck growth of grain boundary between sintered two particles and expressed as a function of porosity. The series structure model with cubic pores explained well the increased tendency of E_c with neck growth rather than the parallel structure model. The thermal conductivity of the three phase system of alumina–mullite–pore was calculated by a theoretical equation developed in this research group, and compared with the experimental results. The pores in the sintered composite were treated as one phase. The measured thermal conductivity of the composite with 0.5–25% porosity (open and closed pores) was in accordance with the theoretical prediction based on the parallel structure model.

Key words : Sintering, Porous ceramics, Thermal conductivity, Thermal expansion

1. Introduction

In a previous paper,[1] a wide variety of thermal conductivity (κ) of metals and ceramics is discussed with a harmonic oscillator model of lattice vibration. The theoretical approach succeeded in representing κ with atomic weight, Young's modulus (E) and density (ρ). The E and ρ values are closely related to the nature of chemical bond (metallic, covalent and ionic bond). A very good agreement is observed between the measured and calculated κ values in the wide range from 1 to 2310 J/smK. The next interesting is the theoretical expression of thermal conductivity for the material with inclusion (second phase or pore). Wang and Pan[2] summarize mixing rules of thermal conductivity for composite materials. The thermal conductivities of two phase systems have been analyzed using parallel model, series model, EMT (effective medium theory) model, Maxwell model, Hamilton model and reciprocity model in their review.[2] The thermal conductivity for a more complex structure with two continuous phases[3] or for a hollow bricks structure[4] is also analyzed. In our previous papers,[5,6] an effective thermal conductivity equation of multiphase systems was theoretically derived. This equation (κ_{ap}) of two phase system can be expressed by three parameters of κ_1 for inclusion, κ_2 for a continuous phase and volume fraction V_1 of inclusion. The newly derived κ_{ap} equation for two phase system was compared with the measured κ_{ap} for the AlN particles-dispersed SiO_2 continuous phase system in our previous paper.[5] A very nice agreement was shown for the measured and calculated κ_{ap} values. Thermal conductivities were also calculated for the refractory brick of carbon–alumina–pore system, carbon–alumina–silicon carbide–pore system and carbon–alumina–silica–pore system.[6] The three or four phase model reflects the microstructure of the refractory brick and predicts the maximum and minimum conductivities in parallel and perpendicular directions to c-axis of graphite. The experimental thermal conductivities were measured in the range predicted from the calculation and very close to the average value of calculated maximum and minimum conductivities.

The desirable mixing rule is to be expressed by less available well known parameters. A model structure of material with simple cubic inclusion, which was used in the calculation of the thermal conductivity of composite,[5] was applied to the derivation of a mixing rule of linear thermal expansion coefficient (TEC) of a composite material.[7] The derived mixing rule was compared with the reported data of the W–MgO system presented in the text book.[8] A very good agreement was shown between the reported and calculated TECs. The newly derived mixing rule was also compared with the reported Turner's equation and Kerner's equation.[8] As compared with the previously developed two equations, the mixing rule in our previous paper was closer to the measured TEC of the W-MgO system. In our recent paper,[7] Young's modulus of the material with simple cubic

†Corresponding author : Yoshihiro Hirata
E-mail : hirata@cen.kagoshima-u.ac.jp
Tel : +81-99-285-8325 Fax : +81-99-257-4742

particulate inclusion was derived and subsequently Young's modulus of the inclusion was treated to be 0 GPa for a porous material. The calculated Young's moduli (parallel and series structure models) for porous alumina compacts were compared with the measured data and explained well the experimental data.[9] This review paper summarizes the above theoretical mixing rules of thermal conductivity, Young's modulus and thermal expansion coefficient for two proposed microstructures with cubic inclusion (Fig. 1 and 2).

2. Model Structures

Figure 1 shows a simple cubic inclusion model with length a in one cubic box with length $1/p$.[5] The number (n) and the volume fraction (V) of cubic inclusion in unit volume of the composite are related by $V = a^3n$. The number (p) of inclusion along one direction of cubic composite is equal to $n^{1/3}$ ($= V^{1/3}/a$) and the distance between two inclusion is given by ($1/p - a$). The structure surrounded by dotted lines (Fig. 1(b)) represents the liner connection of inclusion and matrix. This structure of Fig. 1(b) is sandwiched by two layers of a continuous matrix phase as shown in Fig. 1(c) (unit cell structure). We also treat the model structure in Fig. 1(a) as

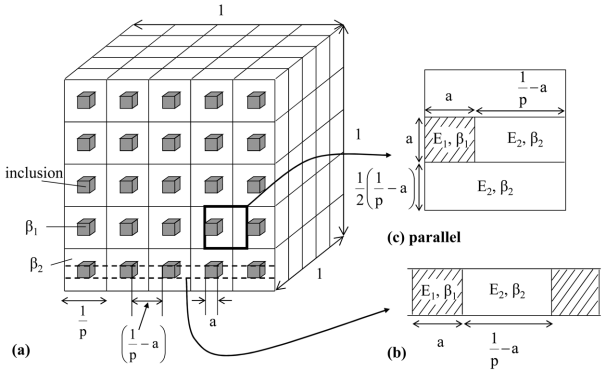

Fig. 1. A parallel model structure of material with simple cubic inclusion with length a. The geometrical features are shown in Fig. 1(b) and (c).

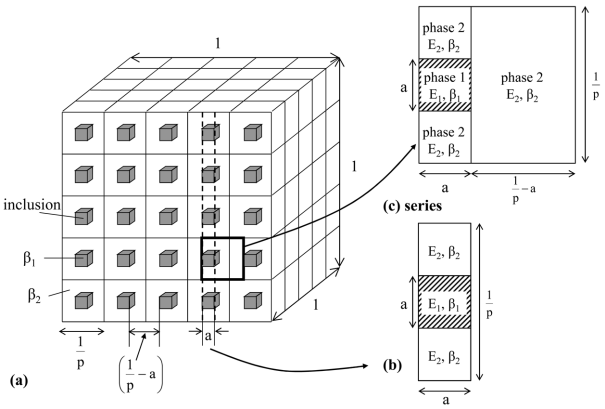

Fig. 2. A series model structure of material with simple cubic inclusion with length a. The geometrical features are shown in Fig. 2(b) and (c).

the connection of rectangular composite (b) and the rectangular continuous phase 2 shown in Fig. 2. The reason why the cubic shape inclusion was employed is that the cubic shape facilitates the calculation of the area mechanically loaded which is required to calculate the Young's modulus and thermal expansion coefficient. The shape and size of inclusions ultimately disappear in the final equation as shown in Tables 1 and 2. Therefore, the presented model equation would be available for obtaining the approximated values in the case of spherical inclusion.

Table 1 summarizes the Young's modulus (E) and thermal expansion coefficient (TEC, β) of a composite in a parallel structure shown in Fig. 1. The derivation of the equations in Table 1 are reported in Ref. 7. We analyze Eq. (1) for the following specific cases.

(a) V = 0

This condition leads to the following relationship: $E_c = E_2$, $\beta_b = \beta_2$, $E_b = E_2$. These relations are substituted for Eq. (1) and result in $\beta_c = \beta_2$. The TEC of composite (c) is equal to that of the continuous phase 2.

(b) $V = 1$

Table 1. Summary of Young's Modulus (E) and Thermal Expansion Coefficient (β) of Composite in a Parallel Structure shown in Fig. 1[7]

$$\beta_c = \frac{E_b V^{2/3}\beta_b + E_2(1-V^{2/3})\beta_2}{E_b V^{2/3} + E_2(1-V^{2/3})} \quad \text{(composite c)} \tag{1}$$

$$E_b = \frac{E_1 E_2}{E_2 V^{1/3} + E_1(1-V^{1/3})} \quad \text{(composite b)} \tag{2}$$

$$\beta_b = \beta_1 V^{1/3} + \beta_2(1 - V^{1/3}) \quad \text{(composite b)} \tag{3}$$

$$\text{Denominator of Eq. (1)} = E_c = E_2 - E_2 V^{2/3}\left[1 - \frac{1}{1 - V^{1/3}\left(1 - \frac{E_2}{E_1}\right)}\right] \tag{4}$$

E_1: Young's modulus of dispersed phase 1
E_2: Young's modulus of continuous phase 2
E_b: Young's modulus of composite (b) in Fig. 1(b)
E_c: Young's modulus of composite (c) in Fig. 1(c)
V: Volume fraction of dispersed phase 1
β_1: Thermal expansion coefficient of dispersed phase 1
β_2: Thermal expansion coefficient of continuous phase 2
β_b: Thermal expansion coefficient of composite (b) in Fig. 1(b)
β_c: Thermal expansion coefficient of composite (c) in Fig. 1(c)

The following relation is derived: $E_c = E_b = E_1$, $\beta_b = \beta_1$. The β_c of Eq. (1) results in $\beta_c = \beta_b = \beta_1$ and is equal to the TEC of dispersed phase 1.

(c) $E_1 = 0$ GPa

This condition means the formation of pores in a continuous phase 2 and leads to the relation of $E_b = 0$.

$$E_c = E_2(1 - V^{2/3}) \quad (5)$$

$$\beta_c = \beta_2 \quad (6)$$

In this case, the Young's modulus of the porous solid decreases as a function of porosity as presented by Eq. (5).[10] However, the TEC of the porous material is independent of porosity and equal to that of the continuous phase.[10] This theoretical prediction is discussed in the latter part.

Eq. (1) is derived for the two phase composite. However, this equation is easily extended to a multiphase system.[6] In the three phase system of dispersed phase 1 (volume fraction V_1), continuous phase 2 (volume fraction V_2) and dispersed phase 3 (volume fraction V_3), we calculate at first the relation summarized in Table 1 for phases 1 and 2. A care is taken to the calculation of volume fraction of phase 1. The V in Table 1 is changed to $V_1 / (V_1 + V_2)$ where $V_1 + V_2 + V_3 = 1$. The phase 3 is dispersed in a new continuous phase where phase 1 is included in the original continuous phase 2.

Table 2. Summary of Young's Modulus (E) and Thermal Expansion Coefficient (β) of Composite in a Series Structure Shown in Fig. 2[7]

$$\beta_c = \left(\frac{E_d}{E_c}\right)\beta_d \quad \text{(composite c)} \quad (7)$$

$$E_d = E_1V^{2/3} + E_2(1 - V^{2/3}) \quad \text{(composite b)} \quad (8)$$

$$\frac{1}{E_c} = \frac{V^{1/3}}{E_d} + \frac{1-V^{1/3}}{E_2} \quad \text{(composite c)} \quad (9)$$

$$\beta_d = \frac{E_1V^{2/3}\beta_1 + E_2(1-V^{2/3})\beta_2}{E_1V^{2/3} + E_2(1-V^{2/3})} \quad \text{(composite b)} \quad (10)$$

E_1: Young's modulus of dispersed phase 1
E_2: Young's modulus of continuous phase 2
E_d: Young's modulus of composite (b) in Fig. 2(b)
E_c: Young's modulus of composite (c) in Fig. 2(c)
V: Volume fraction of dispersed phase 1
β_1: Thermal expansion coefficient of dispersed phase 1
β_2: Thermal expansion coefficient of continuous phase 2
β_d: Thermal expansion coefficient of composite (b) in Fig. 2(b)
β_c: Thermal expansion coefficient of composite (c) in Fig. 2(c)

Therefore, repeating two times the calculation summarized in Table 1 provides the β_c value for three phase system. The calculation in Table 1 is repeated to determine the final β_c, depending on the number of phases included in the composite.

Table 2 summarizes the Young's modulus (E) and TEC (β) of composite in a series structure of composite (b) and phase 2 in Fig. 2.[7] We analyze Eq. (7) for the following specific cases.

(a) $V = 0$

This condition leads to the relationship of $E_d = E_2 = E_c$ and $\beta_d = \beta_2 = \beta_c$. The TEC of composite (a) is equal to that of the continuous phase 2.

(b) $V = 1$

The following relation is derived: $E_d = E_1 = E_c$, $\beta_d = \beta_1 = \beta_c$. That is, the β_c is equal to the TEC of a dispersed phase.

(c) $E_1 = 0$ GPa

This condition means the formation of pores in the continuous phase 2 and leads to the relation.

$$E_d = E_2(1 - V^{2/3}) \quad (11)$$

$$\frac{1}{E_c} = \frac{V^{1/3} + (1-V^{1/3})(1-V^{2/3})}{E_2(1-V^{2/3})} \quad (12)$$

$$\beta_c = \beta_2[V^{1/3} + (1 - V^{1/3})(1 - V^{2/3})] \quad (13)$$

Eq. (11) is same as Eq. (5) and the Young's modulus and the TEC of porous composite (a) change with porosity.

3. Comparison of Reported TEC and Calculated TEC of Composite for W–MgO System

In this section, we compare the calculated TEC with the TEC reported in the W–MgO composite.[8] Fig. 3 shows the reported TEC of W–MgO composite as a function of volume fraction of MgO. MgO has a larger TEC than W. The TEC of the W–MgO composite was calculated in two cases: (1) dispersed MgO phase – continuous W phase system and (2) dispersed W phase – continuous MgO phase system. Both the cases in the parallel structure model (Fig. 1) provide the same E_c and β_c values at a same fraction of MgO, indicating that the distinction of dispersed and continuous phases is not needed and only the fraction of included phase is important to the calculation of TEC of composite. Fig. 3(a) shows the calculated TEC for the W–MgO system. The following values were used in the calculation[11]: $E_1 = 354$ GPa and $\beta_1 = 4.5 \times 10^{-6}$ K^{-1} for W, $E_2 = 310$ GPa and $\beta_2 = 13.5 \times 10^{-6}$ K^{-1} for MgO. The calculated TEC was close to the reported TEC.

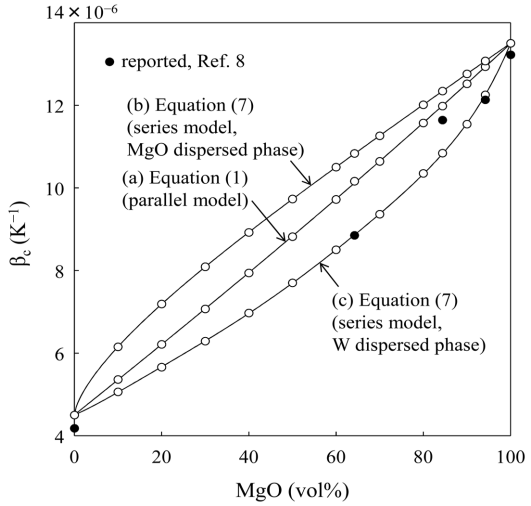

Fig. 3. Thermal expansion coefficient of the W-MgO composite.[7]

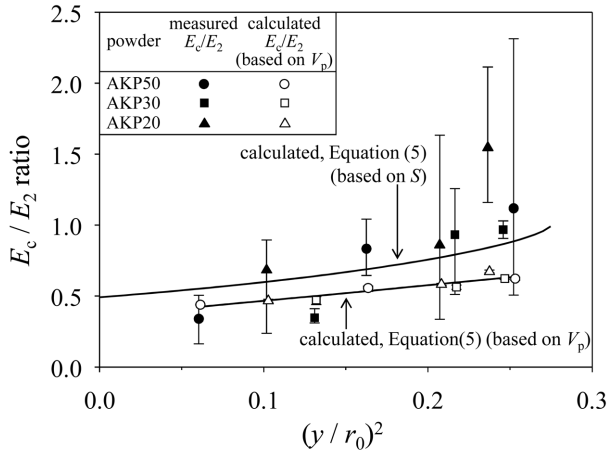

Fig. 4. Comparison of measured and calculated Young's moduli for sintered porous alumina compacts based on a parallel structure of material with simple cubic inclusion.[9]

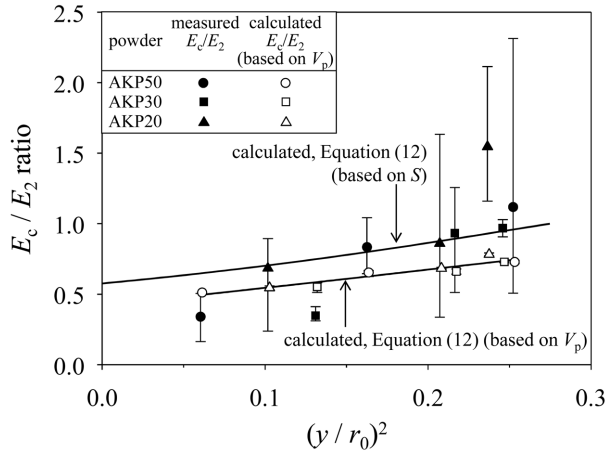

Fig. 5. Variation of Young's modulus of sintered alumina compacts with normalized grain boundary area based on a series structure.[9]

The maximum difference between two TECs was 1.3×10^{-6} K^{-1} at 64.2 vol% MgO.

Figure 3(b) and (c) show the TECs calculated by Eq. (7) for (b) MgO dispersed phase – W continuous phase system and (c) W dispersed phase – MgO continuous phase system, respectively. In Eq. (7), the distinction of the dispersed and the continuous phases provided the different calculated results. As seen in Fig. 3(c), the calculated result showed a very nice correspondence with the reported TEC values. The above comparison suggests that the application of a stress to the series structure shown in Fig. 2(c) explains well the thermal expansion of the composite with particulate inclusion. This model is superior to the parallel structure model shown in Fig. 1(c) for the accurate representation of the TEC of composite. In addition, the comparison of the measured TEC and calculated TEC (Eq. (7)) gives the information of the microstructure related to the dispersed and continuous phases.

4. Young's Modulus of Sintered Porous Alumina Compact

Figures 4 and 5 show the normalized Young's moduli (E_c/E_2, Eqs. (5) and (12)) of sintered alumina compacts as a function of normalized grain boundary area between two sintered particles ($\pi y^2/\pi r_0^2$). The y value is the radius of circular grain boundary and the r_0 value is the radius of initial particles. The detailed analysis of sintering behaviour was reported in our previous papers.[9,12,13] The (y/r_0) ratio was determined from the measured specific surface area (S) for a sintered porous alumina compact. Once the S/S_0 ratio (S_0: specific surface area before sintering) is measured, we can calculate the open porosity (V_p) for a given particle coordination number (n). The measured V_p values decreased nonlinearly with the neck growth ($(y/r_0)^2$) of grain boundary. This tendency was well expressed by the proposed sintering model. To measure the compressive Young's modulus (E_2) for a fully dense alumina compact, the consolidated alumina powder in a graphite mold was hot-pressed at 1500°C for 2 h in an Ar atmosphere. After the hot-pressing, the densified alumina compact was annealed in air at 1000°C for 6 h. The relative density of the dense alumina compact was 99.8%. The measurement of compressive Young's modulus of the dense polycrystalline alumina compact was repeated five times and the average value was 191.8 ± 10.7 GPa. This value was very close to the average stiffness (187 GPa) of single crystal Al_2O_3, reported in our previous paper.[14] The measured Young's modulus was used as a E_2 value in Fig. 4 and 5 to normalize the Young's modulus of the sintered porous alumina compact. As seen in Figs. 4 and 5, the measured E_c/E_2 ratio increased as the neck growth of grain boundary was developed. The increased tendency of E_c/E_2 ratio with neck growth was well represented by the theoretical model curves (Eqs. (5) and (12)) for the calculated and

measured V_p values. The E_c/E_2 ratios by Eqs. (5) and (12) became larger for the V_p value based on S value than for the measured V_p value because of the relationship of V_p based on S < measured V_p. As seen in Figs. 4 and 5, the measured E_c/E_2 ratios were well expressed by Eqs. (12) (series structure model in Fig. 2(c)) rather than Eqs. (5) (parallel structure model in Fig. 1(c)) for the V_p values based on S values. The relatively good agreement between the measured values and calculated values for E_c values in Fig. 5 concludes that (1) neck growth during sintering of spherical particles in a random close packing structure eliminates the pores included in the powder compact, (2) this decrease in the porosity causes increase in the Young's modulus, (3) only the measurement of S value is enough to provide the theoretical prediction of both the V_p and E_c curves for the given n and E_2 values and (4) Eq. (12) for the S-based V_p value is in agreement with the measured E_c values of sintered porous alumina compacts.

5. Thermal Conductivity of the Alumina–mullite–pore System

Eq. (4) in Table 1 and Eq. (9) in Table 2 are the same Eqs. as the thermal conductivities (κ_c) of composites with particulate inclusion when E is changed to κ. In the calculation of κ_c, a flux (J) of energy is input to the composites (Figs. 1 and 2) instead of a stress. As explained in Section 2, the thermal conductivity (κ_b) of three phase system for Fig. 1(c) is expressed by Eq. (14),

$$\kappa_b = \kappa_{ap} - \kappa_{ap} V_3^{2/3} \left[1 - \frac{1}{1 - V_3^{1/3}\left(1 - \frac{\kappa_{ap}}{\kappa_3}\right)} \right] \quad (14)$$

where κ_{ap} is given by Eq. (4) in Table 1 (E is changed to κ) and phase 1 is treated as pore (air) and κ_1 is 0.0265 W/mK at 300 K.[15] Care is to be taken to determine the value of V_1 in three phase system, as discussed in Section 2. Calculation of κ_b was carried out for two cases: Case A – mullite continuous phase (κ_2: 6.07 W/mK at 373 K[16]), Case B – alumina continuous phase (κ_2: 36 W/mK at 300 K[15]). In case A, alumina particles were treated as a dispersed phase 3 in Eq. (14). Similarly, mullite particles were treated as a dispersed phase 3 in case B. When the pore size is less than a molecular mean free path of gas, the thermal conductivity is affected by the pore size. Generally, the pore sizes of a refractory material are larger than the molecular mean free path. Thus, the difference between open and closed pores causes little influence on E, κ and TEC.

Figure 6(a) - (d) show the schematic structures of mullite–alumina–pore system along the κ_b line (parallel structure model) at V_1 (porosity) = 20 vol%. At point (a) (V_3 (alumina) = 0 vol%), pores of V_1 = 20 vol% are dispersed in a mullite continuous phase.[17] The addition of Al_2O_3 particles in a mullite continuous phase, which causes the decrease of volume fraction of mullite phase, increases slightly the κ_b value because of the relationship of κ_{ap} (pore-containing mullite phase) < κ_3 (alumina particles). However, the κ_b value starts to decrease above V_3 = 70 vol% (Fig. 6(c)) and reaches the lowest value at V_3 = 80 vol% where a mullite continuous phase disappears (Fig. 6(d)). In the V_3 range of 70 to 80 vol%, the continuous phase changes from mullite to air and alumina particles with a higher thermal conductivity is separated from another Al_2O_3 particles by air. Therefore, introduction of continuously distributed pores has a significant effect to decrease the κ_b value of dense two phase systems.

Figure 7 shows the measured and calculated thermal conductivities for the alumina–mullite–pore system.[17] The calculation (Eq. (14)) contained the influence of pores. As seen in Fig. 7, a very nice agreement was observed between the measured κ_b value and the calculated κ_b value for a mullite continuous phase. The thermal conductivity of alumina phase with pores was also simulated by the proposed model, which provided the higher thermal conductivities than the measured values. The above comparison of κ_b values sug-

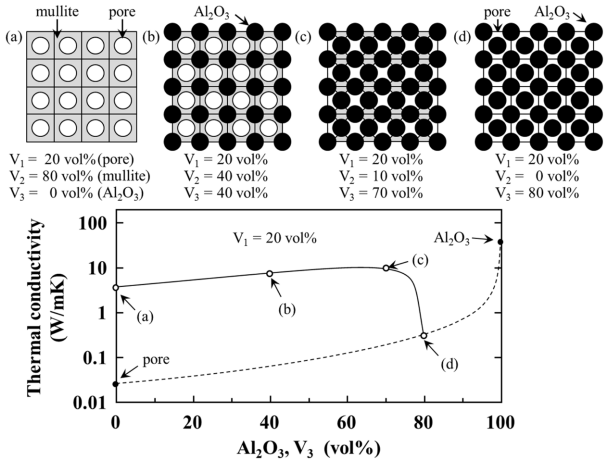

Fig. 6. Relationship between the model structure and the calculated thermal conductivity (Eq. (14)) for alumina–mullite–pore system. V_1: volume fraction of pore; V_2: mullite volume fraction (continuous phase); V_3: alumina volume fraction.

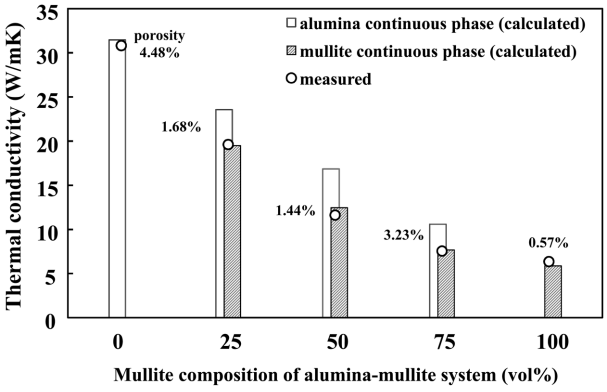

Fig. 7. Comparison of the thermal conductivities between the measurement and the calculation (Eq. (14)) for the alumina–mullite–pore system.[17]

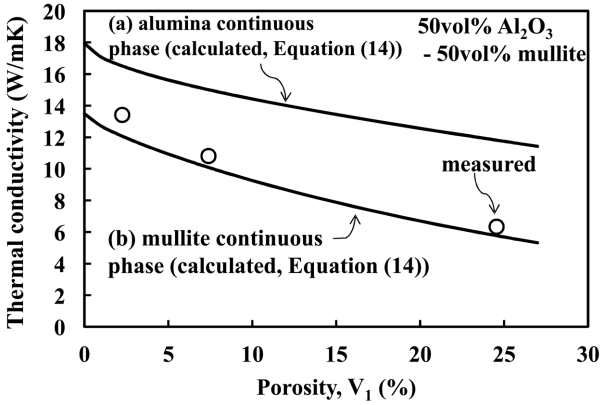

Fig. 8. Effect of the porosity on the thermal conductivity of alumina–mullite–pore system.[17]

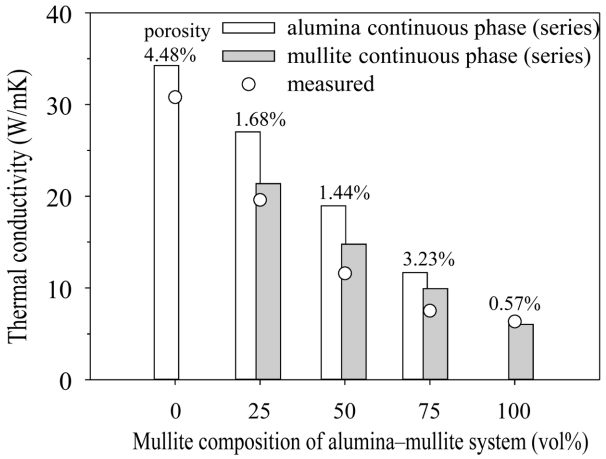

Fig. 9. Measured thermal conductivities of the alumina–mullite–pore system and the calculated thermal conductivities for a series structure (Fig. 2(c), Eq. (15)).

gests that the pores in the alumina–mullite–pore system are included in the mullite continuous phase.

Figure 8 shows the thermal conductivity of 50 vol% alumina–50 vol% mullite system as a function of porosity (open and closed pores). The solid lines indicate the calculated values (Eq. (14)) for (a) the alumina continuous phase and (b) the mullite continuous phase. The measured thermal conductivity is well explained by the calculation for the mullite continuous phase. The proposed thermal conduction model is effective for the composite containing at least 25 vol% porosity. The comparison of measured and calculated κ_b values in Figs. 7 and 8 suggests that the phase with a lower κ value (mullite) can be treated as a continuous phase and provides a significant influence on the thermal conductivity of a composite material.

The thermal conductivity (κ_b) of three phase system for Fig. 2(c) (series structure model) is expressed by Eq. (15),

$$\frac{1}{\kappa_b}=\frac{1-V_3^{1/3}}{\kappa_{ap}}+\frac{V_3^{1/3}}{\kappa_b V_3^{2/3}+(1-V_3^{2/3})\kappa_{ap}} \quad (15)$$

where κ_{ap} is given by Eq. (9) in Table 2 (E is changed to κ) and phases 1, 2 and 3 are treated as dispersed pore, continuous mullite (or alumina) phase and dispersed alumina (or mullite) phase, respectively. Fig. 9 shows the comparison of the measured and calculated thermal conductivities for the alumina–mullite–pore system. As compared with the result in Fig. 7, both the calculated conductivities for alumina continuous phase and mullite continuous phase in the series structure (Fig. 9) became higher than the measured thermal conductivity. That is, the parallel structure model in Fig. 1(c) reflects well the mixing rule of the thermal conductivity for a composite material.

6. Conclusions

The Young's modulus (E) and the linear thermal expansion coefficient (β) of the composite with particulate inclusion were analyzed using two laminate model structures: a parallel structure model of the rectangular composite (series connection of dispersed phase 1 and continuous phase 2) and the continuous phase 2 surrounding the rectangular composite, and a series structure of the rectangular composite (parallel connection of dispersed phase 1 and continuous phase 2) and rectangular continuous phase 2. The newly derived β Eqs. for both the model structures can be represented by β_1 of the inclusion, β_2 of the continuous phase, V of the volume fraction of inclusion, E_1 of the inclusion and E_2 of the continuous phase. The calculated β for the W–MgO composite was compared with the reported β value. The series structure of the composite is superior to the parallel structure model for the correspondence with the measured TEC of the composite. The Young's modulus (E_c) of sintered porous alumina ceramics was also derived from the mixing rule of E_1 of a dispersed phase and E_2 of a continuous phase for the proposed laminated model structure of composite. The series structure model explained well the increased tendency of E_c with neck growth rather than the parallel structure model. A theoretical thermal conductivity (κ_b) of alumina–mullite–pore system was calculated for two cases: mullite continuous phase and alumina continuous phase for the proposed two laminated model structures. In the parallel structure model, a very nice agreement was observed between the measured κ_b value and the calculated κ_b value for the mullite continuous phase. The phase with a lower κ value (mullite) can be treated as a continuous phase and provides a significant influence on the thermal conductivity of a composite material. The theoretical thermal conductivity for the parallel structure model can also explain the porosity dependence of thermal conductivity at least 25 vol% porosity. As compared with the parallel structure model, the calculated κ_b value for the series structure model did not correspond with the measured κ_b value.

REFERENCES

1. Y. Hirata, "Thermal Conduction Model of Metal and Ceramics," *Ceram. Inter.*, **35** 3259-68 (2009).
2. M. Wang and N. Pan, "Predictions of Effective Physical Properties of Complex Multiphase Materials," *Mater. Sci. Eng.,* **R63** 1-30 (2008).
3. J. Wang, J. K. Carson, M. F. North, and D. J. Cleland, "A New Structural Model of Effective Thermal Conductivity for Heterogeneous Materials with Co-Continuous Phases," *Inter. J. Heat Mass Transfer,* **51** 2389-97 (2008).
4. A. Bouchair, "Steady State Theoretical Model of Fired Clay Hollow Bricks for Enhanced External Wall Thermal Insulation," *Building and Environment*, **43** 1603-18 (2008).
5. Y. Hirata, "Representation of Thermal Conductivity of Solid Material with Particulate Inclusion," *Ceram. Inter.*, **35** 2921-26 (2009).
6. Y. Hirata, N. Matsunaga, J. Yoshitomi, and T. Kayama, "Theoretical Analysis of Thermal Conductivity of Graphite-Containing Refractory Brick," *J. Tech. Assoc. Refract. Japan,* **31** [3] 156-63 (2011).
7. Y. Hirata, "Representation of Thermal Expansion Coefficient of Solid Material with Particulate Inclusion," *Ceram. Inter.,* **41** 2706-13 (2015).
8. W. D. Kingery, H. K. Bowen, and D. R. Uhlmann, Introduction to Ceramics; pp. 583-624, Second Ed., John Wiley & Sons, New York, 1976.
9. Y. Hirata and T. Shimonosono, "Theoretical Prediction of Compressive Strength, Young's Modulus and Strain at Fracture of Sintered Porous Alumina Compacts," *Ceram. Inter.*, **42** 3014-18 (2016).
10. D. Hull and T. W. Clyne, An Introduction to Composite Materials; pp. 237-44, Second Ed., Cambridge University Press, Cambridge, 1996.
11. K. Hata, Chemical Handbook, Basic Part II; pp. 21-22, 3rd ed., The Chemical Society of Japan, Maruzen, Tokyo, 1984.
12. Y. Hirata, T. Shimonosono, T. Sameshima, and S. Sameshima, "Compressive Mechanical Properties of Porous Alumina Powder Compacts," *Ceram. Inter.,* **40** 2315-22 (2014).
13. Y. Hirata, T. Shimonosono, S. Sameshima, and H. Tominaga, "Sintering of Alumina Powder Compacts and Their Compressive Mechanical Properties," *Ceram. Inter.*, **41** 11449-55 (2015).
14. Y. Hirata, "Theoretical Analyses of Thermal Shock and Thermal Expansion Coefficients of Metals and Ceramics," *Ceram. Inter.,* **41** 1145-53 (2015).
15. K. Hata, Chemical Handbook, Basic Part II; pp. 72-7, 3rd Ed., The Chemical Society of Japan, Maruzen, Tokyo, 1984.
16. R. F. Davis and J. A. Pask, "Mullite,", pp. 37-75 in High temperature oxide, part IV. Ed. by A.M. Alper, Academic Press, New York, 1971.
17. S. Itoh, Y. Hirata, T. Shimonosono, and S. Sameshima, "Theoretical and Experimental Analyses of Thermal Conductivity of the Alumina-Mullite System," *J. Eur. Ceram. Soc.,* **35** 605-12 (2015).